Chaos-based communications using semiconductor lasers subject to feedback from an integrated double cavity

2008 J. Phys. B: At. Mol. Opt. Phys. 41 155401

(http://iopscience.iop.org/0953-4075/41/15/155401)

J. Phys. B: At. Mol. Opt. Phys. **41** (2008) 155401 (8pp) doi:10.1088/0953-4075/41/15/155401

Chaos-based communications using semiconductor lasers subject to feedback from an integrated double cavity

V Z Tronciu[1,2], Claudio R Mirasso[1] and Pere Colet[1]

[1] Instituto de Física Interdisciplinar y Sistemas Complejos (IFISC) CSIC-UIB, Campus Universitat de les Illes Balears, E-07122 Palma de Mallorca, Spain
[2] Department of Physics, Technical University of Moldova, Chisinau MD-2004, Republic of Moldova

E-mail: vasile@ifisc.uib.es

Received 17 March 2008, in final form 6 June 2008
Published 11 July 2008
Online at stacks.iop.org/JPhysB/41/155401

Abstract
We report the results of numerical investigations of the dynamical behaviour of an integrated device composed of a semiconductor laser and a double cavity that provides optical feedback. Due to the influence of the feedback, under the appropriate conditions, the system displays chaotic behaviour appropriate for chaos-based communications. The optimal conditions for chaos generation are identified. It is found that the double cavity feedback requires lower feedback strengths for developing high complexity chaos when compared with a single cavity. The synchronization of two unidirectional coupled (master–slave) systems and the influence of parameters mismatch on the synchronization quality are also studied. Finally, examples of message encoding and decoding are presented and discussed.

1. Introduction

The synchronization of chaotic oscillators has been the subject of significant studies in the last few years due to its fundamental and applied interests [1]. From the application point of view, chaos-based communications have become an option to improve privacy and security in date transmission, especially after the recent field demonstration of the metropolitan fibre networks of Athens [2]. In optical chaos-based communications, the chaotic waveform is generated by using semiconductor lasers with either all-optical [3–7] or electro-optical [8–10] feedback loops. In particular, semiconductor lasers subject to the influence of optical feedback from a distant mirror have been investigated extensively for the past two decades and different dynamical behaviours have been characterized, including periodic and quasi-periodic pulsations, low frequency fluctuations and coherent collapse (for more details, see [11]). In the conventional all-optical feedback case (COF), the set-up consists of a laser with an external mirror. Typically, to achieve chaotic behaviour in COF a delay roundtrip time of at least few hundreds of picoseconds is needed. So, in air the external cavity should be about few centimetres long, which is a drawback for the design of compact chaotic sources. In this context, multi-section lasers with an amplified feedback section could be suitable candidates for integrated chaotic emitters. Due to the continuing technological progress, multi-section lasers have reach stable and compact configurations which include integrated sections with common waveguides tunable phase shifts [12]. However, the simplest configuration, a two-section laser with one active section and one passive section acting as an external cavity, is not suitable since the length of the passive section is typically too short to achieve chaotic dynamics. Therefore, more complex designs have to be explored. A recent step in this direction was the consideration of integrated three section lasers with amplified feedback [13]. Here we consider a different configuration which includes feedback from an integrated double cavity.

Lasers subject to feedback from two cavities have been considered in several configurations [14–18]. In particular, feedback from a second cavity has been used to control the chaotic dynamics of semiconductor lasers with optical feedback. Control in the low frequency fluctuation regime has been achieved by properly adjusting both the length and the feedback strength of the second external cavity. Configurations using Fabry–Perot resonators to provide feedback have also been studied [19, 20]. In this

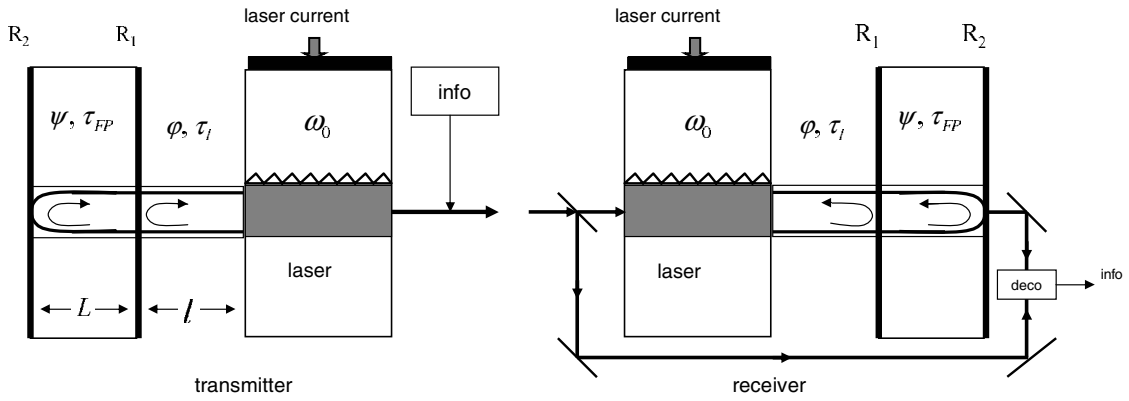

Figure 1. A sketch of the proposed setup for chaos synchronization and message encoding, using semiconductor lasers under the influence of double cavity feedback. R_1 and R_2 are the reflectivity of the air-material facet and the outer facet of the material cavity, respectively. The length of the air cavity l and the material cavity L are taken to be the same: $L = l = 1$ cm, $n_L = 3$; ω_0 is the free running frequency of the CW laser.

case, the feedback can destabilize the laser emission but can also improve the stability of CW emission by enhancing the damping of relaxation oscillations or allowing the control of the chip in a non-invasive way.

In this paper, we consider an integrated device composed of a semiconductor laser subject to feedback from a double cavity with the aim of generating a complex chaotic waveform suitable for applications in chaos-based communications. The scheme of the system is depicted in figure 1. It consists of a single mode semiconductor laser coupled to an external passive cavity of the same III–V material through an airgap. Here we choose the two external cavities (airgap and III–V material) of the same length, in this case 1 cm. To avoid diffraction losses in the air cavity, a microlens should be placed at the laser facet to collimate the beam (not shown in our set-up). Assuming a refractive index of 3 for the material, the total delay time in the two cavities amounts to approximately 0.266 ns. The advantage of this double cavity configuration is the existence of two feedback phases, one in the airgap cavity and the other in the material cavity; the latter can be easily adjusted to destabilize the dynamics of the laser. Moreover, while we assume that the first reflectivity is defined by the air-material facet, the outer facet of the material cavity can be coated to increase its reflectivity. We study the conditions for which the behaviour of the system is chaotic due to the influence on the laser dynamics of the feedback from the double cavity. We also study the synchronization of two of such systems under unidirectional coupling. In the absence of coupling, the behaviour of transmitter and receiver systems is uncorrelated. When a certain amount of light is injected from the transmitter into the receiver, the latter is able to synchronize to the emitter under appropriate conditions. Typically, the receiver does not synchronize identically to the emitter due to the injected field. Therefore, synchronization is not complete but generalized [21]. Synchronization is robust to small perturbations of the carrier. A message of small amplitude can then be included in the carrier which will be filtered out by the receiver. Several message encoding schemes have been proposed in the literature [22, 23]. Here we include the message as a modulation in the amplitude of the chaotic carrier (chaos modulation) [3]. The message can be decoded at the receiver by comparing its input (carrier mixed with message) with its output (which ideally reproduces only the carrier).

The paper is structured as follows. In section 2, we introduce an appropriate model to describe the system dynamics. Section 3 presents a study of the dynamics of a laser under the influence of double cavity feedback (DCF). In section 4, we study the synchronization of two of such systems. The influence of the mismatch in the feedback phases on the synchronization quality is also discussed. Section 5 is devoted to message encoding and decoding. Finally, conclusions are given in section 6.

2. The model

To model the set-up shown in figure 1, we consider a single mode CW laser coupled to a longitudinal double cavity. The first mirror is located at distance l from the laser facet. The distance between first and second mirrors is L. The optical feedback phase in the second cavity ψ can be controlled by injecting current into the passive section. We assume that the current injected in the passive section is small enough to affect only the refractive index, so that the optical length of the resonator is changed in the sub-wavelength range. In this way, while the feedback phase ψ can be tuned, the change in the delay time between the two mirrors τ_L is negligible. Alternatively, this phase could also be controlled with a piezo actuator. In principle, multiple reflections may take place. However, for the feedback parameters we will use, it is enough to consider a single reflection in both cavities. This approximation strongly simplifies the calculations.

The laser dynamics can be analysed in the framework of the extended Lang–Kobayashi equations for the complex field amplitude E and an excess carrier density N [24, 25]:

$$\frac{\mathrm{d}E_{t,r}}{\mathrm{d}t} = (1+\mathrm{i}\alpha)\left[\frac{g(N_{t,r}-N_0)}{1+\varepsilon|E_{t,r}|^2} - \frac{1}{\tau_{\mathrm{ph}}}\right] \times \frac{E_{t,r}}{2} + \gamma_{t1,r1}\,\mathrm{e}^{-\mathrm{i}\varphi}E_{t,r}(t-\tau_l) + \gamma_{t2,r2}\,\mathrm{e}^{-\mathrm{i}(\varphi+\psi)} \times E_{t,r}(t-(\tau_l+\tau_L)) + k_r E_t, \quad (1)$$

$$\frac{dN_{t,r}}{dt} = \frac{I_{t,r}}{e} - \frac{1}{\tau_e}N_{t,r} - \frac{g(N_{t,r}-N_0)}{1+\varepsilon|E_{t,r}|^2}|E_{t,r}|^2. \quad (2)$$

The subscripts t and r refer to transmitter and receiver lasers, respectively. The last term in equation (1) is present only in the receiver laser and describes the unidirectional coupling. k_r is the coupling parameter of the injected field into the receiver laser given by $\kappa_r = \sqrt{1-R}\eta_{\text{ext}}/(\tau_c\sqrt{R})$, where R is facet power reflectivity of the slave laser ($R = 30\%$), τ_c is the cavity roundtrip time of the light within the laser ($\tau_c = 10$ ps), η_{ext} accounts for losses different than those introduced by the laser facet ($\eta_{\text{ext}} = 0.5$). τ_l and τ_L are the airgap and passive material roundtrip times, respectively. $\gamma_{t1,r1}$ and $\gamma_{t2,r2}$ are the feedback strengths governed by the reflectivity R_1 and R_2, respectively. For simplicity, we assume R_1 and R_2 such that $\gamma_{t1} = \gamma_{t2} = \gamma_{r1} = \gamma_{r2} = \gamma$. $\varphi = \omega_0\tau_l$ (whose value can strongly vary from one device to another) and $\psi = \omega_0\tau_L$ are the optical phase accumulated in the airgap and material cavities, respectively. The other parameter values are $\alpha = 5$, the linewidth enhancement factor; $g = 1.5 \times 10^{-8}$ ps^{-1}, the differential gain parameter; $\varepsilon = 5 \times 10^{-7}$, the gain saturation coefficient; $\tau_{\text{ph}} = 3$ ps and $\tau_e = 2$ ns, the photon and carrier lifetimes, respectively; $\tau_l = 0.066$ ns and $\tau_L = 0.2$ ns, the round trip times. The injected current is fixed at $I = 50$ mA (the threshold current $I_{\text{th}} = 11.5$ mA) and the carrier number at the transparency at $N_0 = 1.2 \times 10^8$. The parameter values are used for the calculated results that are shown in all figures of the paper.

3. Laser dynamics under the influence of double cavity feedback

3.1. Stationary states. External cavity modes

In the subsequent analysis, we consider the stationary lasing states of the system (1) and (2). They are given by rotating wave solutions, usually called external cavity modes (ECMs),

$$E(t) = E_S\, e^{i\omega_S t}, \qquad N = N_S. \quad (3)$$

Inserting (3) into (1) and (2), we obtain a transcendental equation for the emission frequency ω_S:

$$\begin{aligned} F(\omega_S) = &-\omega_S + \alpha\gamma[-\cos(\varphi+\omega_S\tau_l) \\ &- \cos(\varphi+\psi+\omega_S(\tau_l+\tau_L)] - \gamma[\sin(\varphi+\omega_S\tau_l) \\ &+ \sin(\varphi+\psi+\omega_S(\tau_l+\tau_L))], \end{aligned} \quad (4)$$

where ω_S is obtained from $F(\omega_S) = 0$. Finally, E_S and N_S can be obtained by inserting the value of ω_S in (1) and (2) and equalling rhs to zero.

When only one cavity is present (COF), equation (4) provides a finite number of solutions which are located on top of an ellipse in the N_S versus ω_S plane. This elliptical locus for the solutions is independent of the feedback phase $\omega_S\tau$, τ being the external cavity roundtrip time. The feedback phase then determines the exact number of solutions as well as its precise location on the ellipse. If the feedback phase is changed, the location of the solutions moves on the ellipse.

In contrast to the COF case, the feedback from the Fabry–Perot resonator implies a non-elliptic location of modes [19]. For different phases φ, the location of the ECMs moves along an eight-shape figure, with the solitary laser mode located in the waist. The nature of the bifurcations and the stability of the solutions for the resonant feedback from FPR have been analysed in more detail in [19].

The situation is again different for the case of DCF. The solid lines in figures 2(c) and 3 show the locus of ECMs in the plane ($N_S - \omega_S$) for two different levels of feedback strength and different values of one of the feedback phases φ. The other feedback phase, ψ, then determines the exact number of solutions and its precise location on the geometrical locus (marked by circles). We first consider a small feedback strength $\gamma = 5$ ns^{-1} (left column in figure 2(c)). For $\varphi = -\pi/2$, the location of the fixed points is similar to that of the COF case, i.e. the modes are located on a ellipse although now the ellipse is distorted (see figure 2(c) (left)). The number of ECMs depends on the values of the feedback phase. Only one mode is present for $\psi = \pi/4$. When the feedback strength is increased to $\gamma = 15$ ns^{-1} (right column in figure 2(c)), new satellite bubbles of ECMs appear on left and right sides of the deformed ellipse. The different satellite bubbles span for a range of frequencies which is much larger than for the weak feedback case $\gamma = 5$ ns^{-1}. The onset of these bubbles reflects the existence of frequency gaps for which no ECM solutions exist. These frequency gaps are originated from destructive interference in the feedback coming from the two cavities. Figure 2(a) shows the total reflected light for $\gamma = 5$ ns^{-1} (left) and $\gamma = 15$ ns^{-1} (right). For the last value of γ within the range of frequencies in which ECM solutions are found, there are two regions of vanishing reflected light which correspond to the two regions that separate the three bubbles shown in the right panel of figure 2(c)). Figure 2(b)) shows the value of the rhs of equation (4) for $\varphi = -\pi/2$. It can be seen as a fast oscillatory behaviour on top of a slower one. The fast and slow oscillatory periods are determined by the two feedback times. The intersection of this curve with zero shows the solutions of equation (4). Increasing γ, the amplitude of the oscillations becomes larger and therefore more ECMs exist for any given values of the feedback phases. Also increasing the feedback strength leads to the emergence of additional bubbles of ECMs. For $\varphi = \pi/6$, the system exhibits almost the tilted eight-shape (see figure 3(a) (left)) which is similar to that found in a Fabry–Perot resonator [19]. Although the level of feedback is still the same as before, the number of solutions has increased for $\psi = \pi/4$. Also note that the size of the locus for the ECMs is clearly larger than in the previous case. Finally, for $\varphi = \pi/2$ the tilted eight-shape opens in the centre leading to a 'peanut' shape for the locus of the ECMs (see figure 3(b) (left)). The overall size of the locus as well as the approximate number of solutions is the same as for $\varphi = \pi/6$. This clearly illustrates that in the case of the DCF, the location of the modes becomes more complicated when compared with that of the COF.

3.2. Chaotic behaviour

For feedback strength small enough, a laser under the influence of COF or DCF shows either CW or pulsating operation. Chaotic behaviour appears as the feedback strength

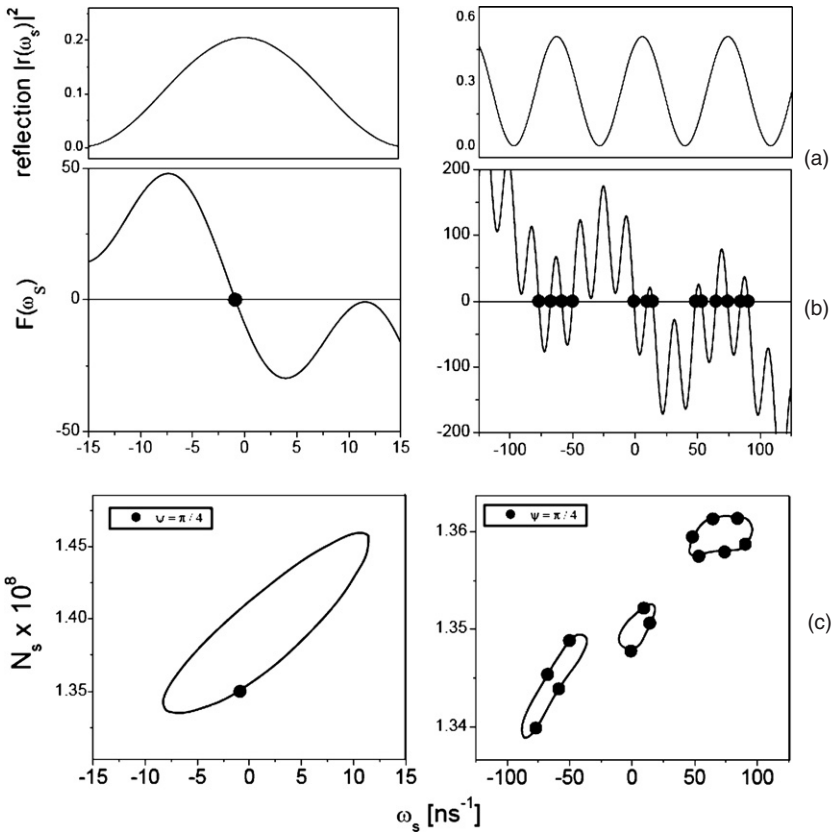

Figure 2. External cavity modes for a double cavity with $\gamma = 5$ ns^{-1} (left) and $\gamma = 15$ ns^{-1} (right). (a) Reflection spectrum. (b) Graphical solution of (4) for $\varphi = -\pi/2$ and $\psi = \pi/4$. The circles indicate the modes. (c) Locus of the ECMs in the plane $(N_S - \omega_S)$ for $\varphi = -\pi/2$. The circles indicate the precise location of ECMs for the feedback phase $\psi = \pi/4$.

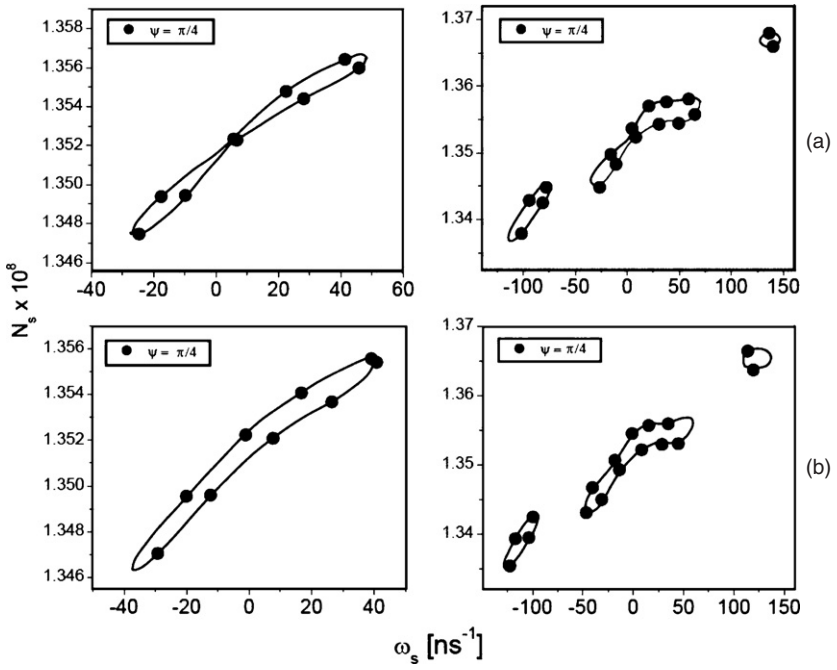

Figure 3. Locus of the ECMs in the plane $(N_S - \omega_S)$ for different phases. (a) $\varphi = \pi/6$ and (b) $\varphi = \pi/2$ and two levels of feedback strength: $\gamma = 5$ ns^{-1}, (left) and $\gamma = 15$ ns^{-1} (right). The symbols indicate the external cavity modes for $\psi = \pi/4$.

is increased. Figure 4 illustrates typical time traces (left) and the power spectra (right) of a semiconductor laser under the influence of COF and DCF for identical laser parameters in the chaotic regime. It can be observed that the DCF makes the laser behaviour more complex. This fact was further confirmed by calculation of the autocorrelation time from equations (3) $T_c =$

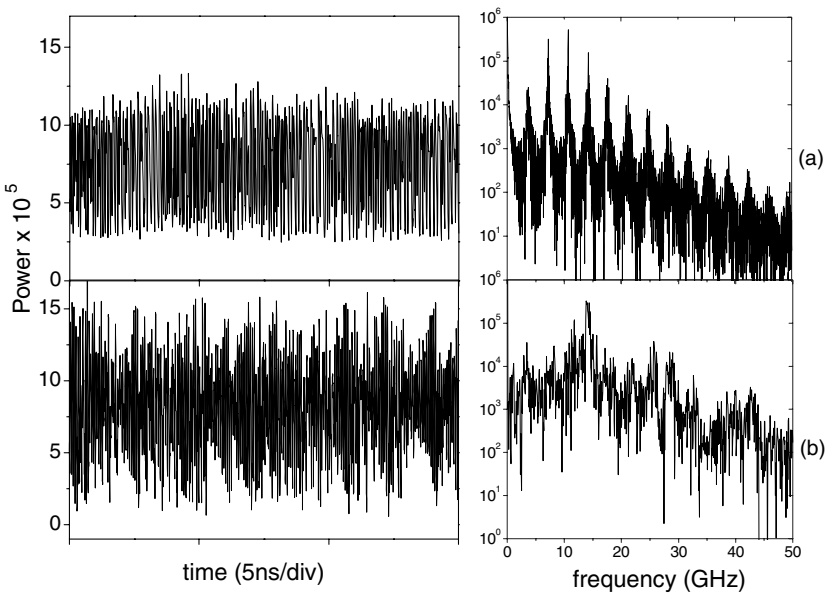

Figure 4. A typical optical power time trace (left) and the power spectrum (right) of a semiconductor laser under the influence of (a) COF for $\gamma = 30\ \text{ns}^{-1}$, $\varphi = -\pi/2$, $\tau = 0.266$ ns and (b) DCF for $\gamma_1 = \gamma_2 = 30\ \text{ns}^{-1}$, $\varphi = -\pi/2$, $\psi = \pi$, $\tau = \tau_l + \tau_L = 0.266$ ns, $\tau_l = 0.066$ ns, $\tau_L = 0.2$ ns.

$\int_0^\infty \mathrm{d}\tau\ \Gamma_{ii}^2(\tau)$ and (4) $\Gamma_{ij}(\tau) = \frac{\langle (P_i(t)-\langle P_i\rangle)(P_j(t-\tau)-\langle P_j\rangle)\rangle}{\sqrt{\langle (P_i(t)-\langle P_i\rangle)^2\rangle \langle (P_j(t)-\langle P_j\rangle)^2\rangle}}$ of [13]. These calculations yield to $T_c^{\text{COF}} \sim 0.1$ ns and $T_c^{\text{DCF}} \sim 0.037$ ns. Moreover, larger amplitude fluctuations when compared with COF can be observed.

Figure 5 displays the bifurcation diagrams of the semiconductor laser subject to DCF for two feedback phases. As the feedback strength is increased, several instabilities take place. For a given value of the feedback strength, the figure displays the values of all the local maxima of the time traces of the emitted power. Considering $\varphi = -\pi/2$ and $\psi = \pi$, for low values of the feedback strength, the CW operation is observed, which is depicted as a single value for the maxima of the power in figure 5(a). At the feedback strength $\gamma = 10\ \text{ns}^{-1}$, Hopf bifurcation appears and the output power develops an oscillatory behaviour. Since the oscillations are periodic, for a given feedback strength all the local maxima of the output power have the same value and consequently a single point appears in figure 5. The Hopf bifurcation is supercritical and, as expected, the oscillation amplitude grows with the square root of the distance from the bifurcation point. As the feedback strength is further increased, a scenario compatible with the quasiperiodic route to chaos is obtained. However, the range and amplitude of this behaviour are small. When the feedback strength reaches the value $\gamma = 15\ \text{ns}^{-1}$, a jump to a new P periodic operation region is observed. As the feedback strength increases, a second scenario compatible with the quasiperiodic route to chaos appears. For large values of the feedback strength, the system displays a chaotic behaviour.

For $\varphi = \pi/2$ and $\psi = \pi/4$ (see figure 5(b)), the system behaviour is slightly different; the Hopf bifurcation is shifted to a lower feedback level involving the appearance of low amplitude chaotic behaviour for low feedback strengths

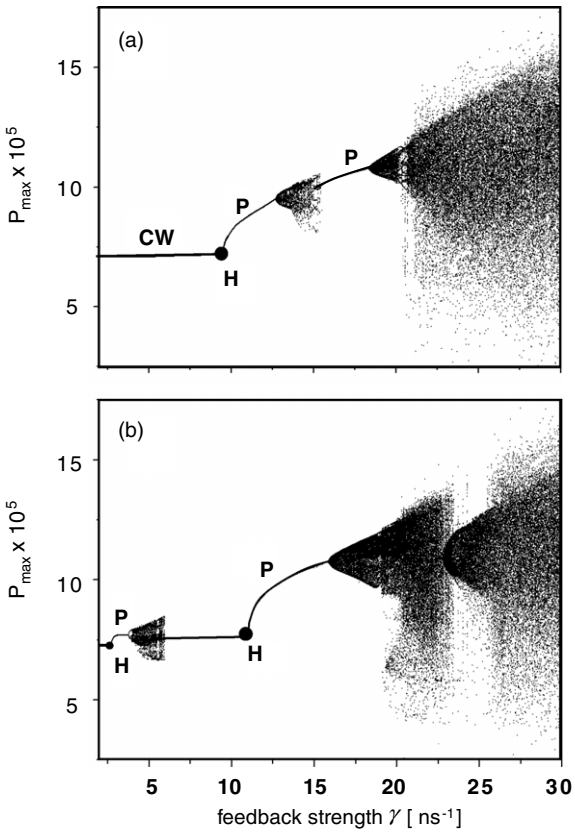

Figure 5. Numerical bifurcation diagrams for different values of phases (a) $\varphi = -\pi/2$, $\psi = \pi$ and (b) $\varphi = \pi/2$, $\psi = \pi/4$. CW shows the continuous-wave operation, the circle H indicates Hopf bifurcation and P shows the peak of the stable periodic solution.

followed by the CW operation and a scenario compatible with the quasiperiodic route to chaos. We mention that the

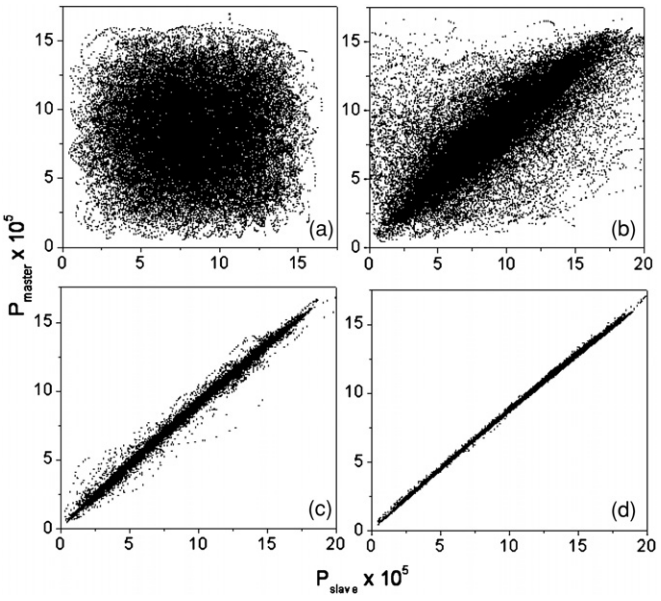

Figure 6. (a) Synchronization diagrams for different levels of the coupling parameter k. (a) $k = 0$ ns^{-1} (the systems are uncorrelated), (b) $k = 50$ ns^{-1} ($C = 0.75$), (c) $k = 75$ ns^{-1} ($C = 0.997$), (d) $k = 100$ ns^{-1}($C = 0.9995$). The feedback strength is taken as $\gamma = 30$ ns^{-1} and the feedback phases are $\varphi = -\pi/2$ and $\psi = \pi$.

numerical calculations show that in this parameter region and for any value of the feedback strength larger than 25 ns^{-1} and combination of phases φ and ψ, the laser behaviour is chaotic and robust.

4. Synchronization and mismatch in feedback phases

In the previous section, we have clarified different aspects of the dynamics of a semiconductor laser with integrated DCF for obtaining chaotic behaviours. In what follows, we are interested in the transmitter–receiver configuration and in the evaluation of its synchronization properties. Synchronization can be quantified by measuring the cross correlation coefficient:

$$[C = \langle P_m(t)P_s(t)\rangle/(\langle|P_m(t)|\rangle\langle|P_m(t)|\rangle)]. \qquad (5)$$

Figure 6 shows the emitted power of the slave system versus the power of the master (synchronization diagram) for feedback strength $\gamma = 30$ ns^{-1}and different levels of the coupling parameter k. We first consider the case of identical master and slave systems, so we take the same parameter values for both of them. When the coupling parameter is equal to zero, as shown in figure 6(a), the trajectories of the master and slave lasers depart from each other and the synchronization map is a cloud of points showing the lack of correlation between outputs. Increasing the coupling parameter to $k = 50$ ns^{-1}, the synchronization map shows a clear synchronization process (see figure 6(b)) with a cross correlation coefficient $C = 0.75$. By increasing the coupling until 100 ns^{-1}, the synchronization improves and the cross correlation coefficient increases approaching 1 (see figures 6(c) and (d)).

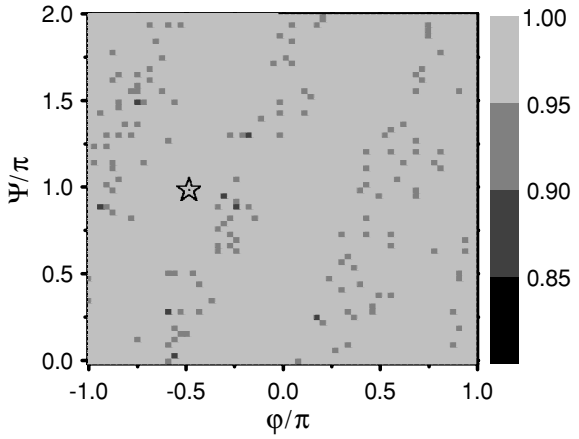

Figure 7. The cross correlation coefficient as a function of the feedback phases for $\gamma = 30$ ns^{-1} and $\kappa = 75$ ns^{-1}. The star is the operating point for message encoding and decoding used in section 5.

Figure 7 shows the dependence of the synchronization quality as a function of the feedback phases. It displays the value of the correlation function in the parameter space $(\varphi - \psi)$ for feedback strength $\gamma = 30$ ns^{-1} and coupling coefficient $\kappa = 75$ ns^{-1}. It can be clearly seen that the region of high correlation coefficients is wide while regions of low correlation hardly appear. The star in figure 7 corresponds to the operating point that will be considered for message encoding and decoding in the following section.

It is well known that the quality of the synchronization depends on the similarity between master and slave lasers. The influence of the internal laser parameters' mismatch on the synchronization quality has been studied in [26, 27], so here we focus on the influence of the mismatch on the two feedback phases. Figure 8 shows the dependence of the cross correlation coefficient on the phase difference (phase master − phase slave) for feedback strength $\gamma = 30$ ns^{-1} and coupling strengths $k = 75$ ns^{-1} (a) and $k = 100$ ns^{-1} (b). The solid line shows the degradation of the synchronization due to a mismatch in the material cavity feedback phase. We take $\varphi_m = \varphi_S = \pi$ and $\psi_s = 0$ while ψ_m is varied from 0 to π. The dotted line shows the effect of a mismatch in the air cavity feedback phase. We consider $\psi_s = \psi_m = \pi$ and $\varphi_S = 0$ while φ_m is varied from 0 to π. When the feedback phases coincide, the system shows perfect synchronization with a $C \sim 1$ cross-correlation coefficient. An increase of the mismatch in any of the feedback phases induces degradation of the synchronization which is indicated by a reduction of the cross correlation coefficient. For small mismatch, the degradation of the correlation is similar for the mismatch in any of the two phases. As the mismatch is increased, the degradation is clearly more severe in the case of mismatch in the feedback phase of the air cavity, φ. This may be understood from the fact that φ is the phase of the shorter cavity and in general short cavities are more sensitive to phase variations than long cavities. For larger values of the coupling strength, the effect of the mismatch in the feedback phases is smaller and therefore the cross-correlation coefficient decreases slower as

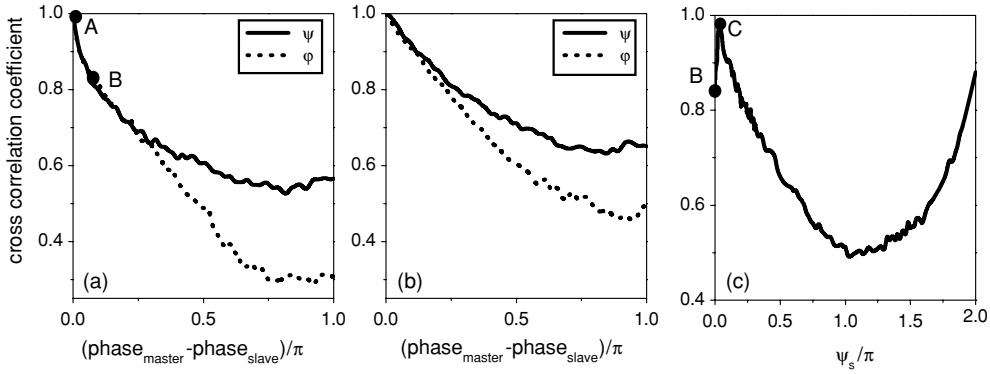

Figure 8. The cross correlation coefficient as a function of the feedback phase difference (phase master − phase slave) for coupling $k = 75$ ns^{-1} (a) to $k = 100$ ns^{-1} (b). Panel (c) shows the cross correlation coefficient for $\varphi_m = \varphi_S = \pi$ and $\psi_m = 0$ as a function of the material phase for the slave laser ψ_s. For both master and slave systems, the feedback strength has been taken as $\gamma = 30$ ns^{-1}.

the mismatch is increased. High values of the cross-correlation coefficient are usually required for efficient message encoding and decoding; therefore, the mismatch in the feedback phases should not exceed $0.1/\pi$. Alternatively, a small airgap phase mismatch can be compensated adjusting the material phase ψ of the slave laser. Figure 8(c) shows an example of such compensation. The mismatch in the airgap phase is 2.5% (point B of figure 8(a)), and a very good correlation can be achieved (point C).

5. Message transmission

In this section, we consider the use of these integrated devices for message encoding and decoding in chaos-based communications. Several ways for encoding and decoding a message within the chaotic carrier has been proposed in the literature, including chaos modulation [3], chaos shift keying [28], chaos masking [26], etc. Here we consider the chaos modulation technique [3] which can be easily implemented in real devices. The message is encoded as a small amplitude modulation of the emitted field of the master, so that the signal transmitted to the receiver is

$$E_T = E_t(1 + \varsigma m(t)), \tag{6}$$

where $m(t)$ is the message and ς is the message amplitude. At the receiver system, the message is decoded comparing the input of the receiver with its output which is ideally synchronized to the carrier

$$M_{\text{decoded}} = \sqrt{P_T/P_S} - 1. \tag{7}$$

Figure 9 illustrates the transmission of a non-return to zero pseudorandom message. The system parameters correspond to the operating point shown with a white star in figure 7. Panel (a) shows the input message. Panels (b) and (c) show the chaotic carrier without the message and the transmitted signal (carrier with message) respectively. Panel (d) shows the decoded message, as indicated in equation (7), and filtered by an appropriate low-pass filter [29]. As can be seen from the figure, the message is well recovered. Panel (e) shows the recovered message for a 2.5% mismatch in the airgap phases between master and slave lasers. It can be clearly seen

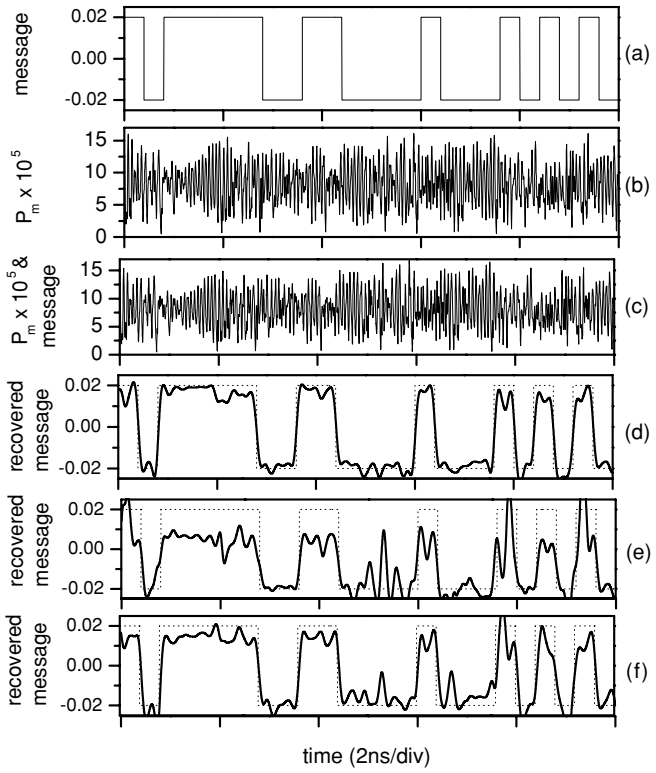

Figure 9. Numerical results of encoding and decoding of a 2.5 Gbit s^{-1} digital message for a closed loop scheme: (a) encoded message, (b) output of the master laser, (c) output of the master laser with a message, (d) recovered message after filtering (solid line) and input message (dotted line) for identical parameters for master and slave lasers (point A of figure 8(a)), (e) recovered message (solid line) after filtering for lasers with 2.5% mismatch of airgap phases (point B of figure 8(a)), (f) recovered message (solid line) after filtering for lasers with 2.5% mismatch of airgap phases, but the slave airgap phase is compensated by a different ψ_s phase (point C of figure 8(c)). Parameters $\gamma = 30$ ns^{-1}, $\kappa = 75$ ns^{-1}, $\varphi = -\pi/2$, $\psi = \pi$, $\tau_l = 0.066$ ns, $\tau_L = 0.2$ ns.

that part of the message cannot be recovered. On the other hand, the airgap phases' mismatch can be compensated by the controllable phase of the slave laser. As can be seen in panel (f), the message is now well recovered.

It is worth to stress that these simple examples of the chaos modulation encoding technique, within a chaotic waveform, obtained from a double cavity feedback are efficient and simple and could be easily applied to a chaos-based communication system by using an external modulation.

6. Summary and conclusions

We have studied the dynamics of an integrated device composed of a semiconductor laser and a double cavity that provides delayed optical feedback. The double cavity feedback implies the existence of two feedback phases which can play an important role in the dynamics. This extra degree of freedom leads to a more complex behaviour which, in fact, is already indicated when looking for the number and location of the fixed points. While in the more conventional case of using a single cavity, these steady states are located on top of an ellipse in the $(N_S - \omega_S)$ plane, in the double cavity case the ellipse can be strongly distorted and can break into several bubbles. The number of coexisting steady states is also increased in the case of double cavity feedback, and chaotic behaviour is found for lower values of the feedback strength. Furthermore, chaos already appears for quite short cavities, allowing for compact devices.

We have shown that two of these devices can be synchronized when operating in the chaotic regime in a master–slave configuration. However, synchronization is degraded when there is a mismatch in the parameters of the master and slave systems. Since the novelty of this scheme is the existence of two feedback phases, we have addressed in detail the effect of a mismatch in these phases. A mismatch in the airgap feedback phase turns out to have stronger effects in the master–slave cross-correlation than a mismatch in the material cavity feedback phase. However, for small enough mismatches, good quality synchronization is achieved. For the parameter values where good synchronization is achieved, it is possible to encode a message in the carrier using the chaos modulation technique. The message can be appropriately recovered at the receiver even for high bit rates. The codification method we employed is just an example of what can be done. While this codification technique is efficient and simple to implement, other codification methods could be used as well. We believe that our work provides a good basis for future study and, in particular, provides some pointers for more detailed investigations of multi-section integrated devices and their applications for chaos-based communication systems.

Acknowledgments

The authors acknowledge financial support from the European commission project Picasso IST-2005-34551 and from Spanish MEC and FCDU under projects TEC 2006-10009/MIC (PhoDECC) and FIS2004-00953 (CONOCE2) and the Technical University of Moldova project 307b/s. They thank Ingo Fischer for useful discussions. VZT expresses his gratitude for the hospitality in the group IFISC at the UIB.

References

[1] Pikovsky A, Rosenblum M and Kurths K 2003 *Synchronization: A Universal Concept in Nonlinear Sciences* (Cambridge: Cambridge University Press)
[2] Argyris A *et al* 2005 *Nature* **438** 343
[3] Mirasso C R, Colet P and Garcia-Fernandez P 1996 *IEEE Photon. Technol. Lett.* **8** 299
[4] Annovazzi-Lodi V, Donati S and Scire A 1996 *IEEE J. Quantum Electron.* **32** 953
[5] Sivaprakasam S and Shore K A 1999 *Opt. Lett.* **24** 466
[6] Fischer I, Liu Y and Davis P 2000 *Phys. Rev.* A **62** 011 801
[7] Bogris A, Kanakidis D F, Argyris A and Syvridis D 2005 *IEEE J. Quantum Electron.* **41** 469
[8] Tang S and Liu J M 2001 *Opt. Lett.* **26** 596
[9] Gastaud N *et al* 2004 *Electron. Lett.* **40** 898
[10] Lin F Y and Tsai M C 2007 *Opt. Express* **15** 302
[11] Krauskopf B and Lenstra D (ed) 2000 Fundamental issues of nonlinear laser dynamics *AIP Conf. Proc.* p 548
[12] Bauer S *et al* 2004 *Phys. Rev.* E **69** 016206
[13] Perez T *et al* 2006 *IEEE Photon. Technol. Lett.* **18** 2135
[14] Simmendinger C and Hess O 1996 *Phys. Lett.* A **216** 97
[15] Ruiz-Oliveras F R and Pisarchik A N 2006 *Opt. Express* **14** 12859
[16] Liu Y and Ohtsubo J 1997 *IEEE J. Quantum Electron.* **33** 1163
[17] Rogister F *et al* 1999 *Opt. Lett.* **24** 1218
[18] Rogister F *et al* 2000 *Opt. Lett.* **25** 808
[19] Tronciu V Z *et al* 2006 *Phys. Rev.* E **73** 046205
[20] Schikora S *et al* 2006 *Phys. Rev. Lett.* **97** 213902
[21] Raúl V, Pérez T and Mirasso C R 2002 *IEEE J. Quantum Electron.* **38** 1197
[22] Ohtsubo J 2002 *IEEE J. Quantum Electron.* **38** 1141
[23] VanWiggeren G D and Roy R 1998 *Science* **279** 1198
[24] Lang R and Kobayashi K 1980 *IEEE J. Quantum Electron.* **16** 347
[25] Mirasso C R, Mulet J and Masoller C 2002 *IEEE Photon. Technol. Lett.* **14** 456
[26] Mirasso C R 2000 Applications of semiconductor lasers to secure communications *Int. Spring School on Fundamental Issues of Nonlinear Laser Dynamics* vol 548, p 112–27
[27] Rogister F *et al* 2002 *Opt. Commun.* **207** 295
[28] Heil T *et al* 2002 *IEEE J. Quantum Electron.* **38** 1162
[29] Sanchez-Diaz A *et al* 1999 *IEEE J. Quantum Electron.* **35** 292